Numerical study of a nonlocal model for water-waves with variable depth

P. Aceves-Sánchez, A.A. Minzoni, P. Panayotaros *

Departamento de Matemáticas y Mecánica, IIMAS-UNAM, Apdo. Postal 20-726, 01000 México, DF, Mexico

ARTICLE INFO

ABSTRACT

We study numerically the propagation of solitary waves in a Hamiltonian nonlocal shallow water model for bidirectional wave propagation in channels of variable depth. The derivation uses small wave amplitude and small depth variation expansions for the Dirichlet–Neumann operator in the fluid domain, and in the long wave regime we simplify the nonlinear and bottom topography terms, while keeping the exact linear dispersion. Solitons are seen to propagate robustly in channels with rapidly varying bottom topography, and their speed is predicted accurately by an effective equation obtained by the homogenization theory of Craig et al. (2005) [7]. We also study the evolution from peaked initial conditions and give evidence for solitary waves with limiting peakon profiles at an apparent threshold before blow-up.

© 2012 Elsevier B.V. All rights reserved.

1. Introduction

The evolution of gravity water waves has been studied for many years and one common strategy is to use approximate simplified equations. One standard approximation is the Boussinesq system for small amplitude long waves, which can be further used to derive unidirectional models such as the KdV equation. The KdV equation and related models describe successfully many salient features of long wave propagation such as solitary waves and their interactions. Unidirectional models with nonlocal terms, such as the one due to Whitham [1], can also describe breaking waves, and cusped solutions of largest height (reminiscent of the cusped Stokes waves). Several authors, Johnson [2], Miles [3], Iguchi [4], Chazel [5], among others, have included the effect of smooth, slowly varying, and step bottom topographies in shallow water theory, while Rosales and Papanicolaou [6], have also studied the effect of a rough bottom on the propagation of solitons using an homogenization approach.

Recently, Craig et al. [7], have reconsidered the problem of long waves using expansions in nonlocal operators valid for arbitrary bottom topography. The end result is a Hamiltonian formulation in terms of pseudodifferential operators that can be calculated recursively in terms of the shape of the wave and the depth variation. In the present work we use a simplified version of this formulation, deriving shallow water equations for bottom topographies with small depth variation. The resulting Boussinesq-type equation is expected to be ill-posed, as in the constant depth case, and we instead work with a system containing the exact (constant depth) linear dispersive term and simplified nonlinear and variable depth terms. The model can be thought of as a bidirectional analogue of the Whitham equation. The use of such simplified systems for shallow water waves was also suggested by Zakharov [8].

We present the results of numerical simulations of the nonlocal Boussinesq–Whitham system we derive in several situations involving constant and variable depth. Smooth initial wave amplitude profiles with suitable unidirectional

---

* Corresponding author. Tel.: +52 5556223600; fax: +52 5556223364.

E-mail addresses: shilambala@hotmail.com (P. Aceves-Sánchez), tim@mym.iimas.unam.mx (A.A. Minzoni), panos@mym.iimas.unam.mx (P. Panayotaros).
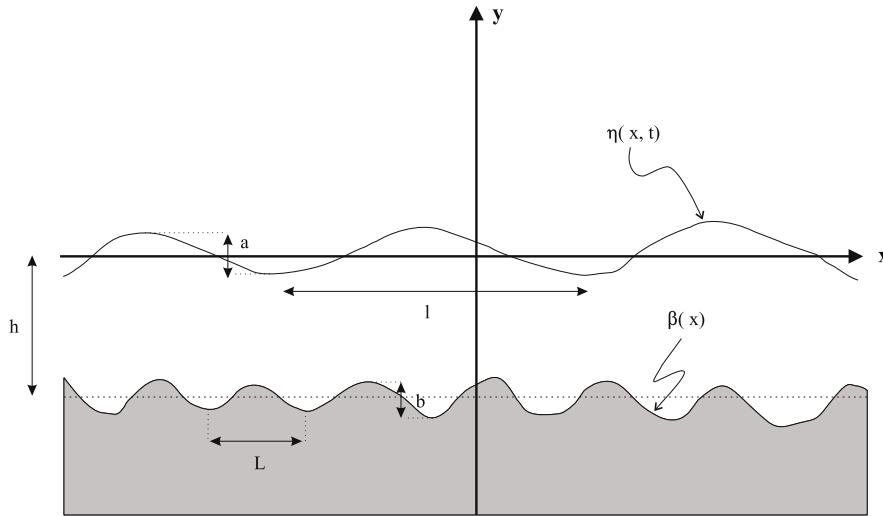
Fig. 1.

velocity potentials lead to KdV-like behavior, with soliton elastic collisions. Smooth step-like depth variations lead to reflected waves of negligible amplitude. Rapidly varying bottom topography produces reflected waves of higher amplitude, however solitons still propagate robustly through the variable depth region without significant change. The main effect is a change of the linear propagation speed, and we see that this change can be predicted accurately by the simple homogenization proposed by Craig et al. [7]. The idea is to use multiscale expansions of integrals to approximate the Hamiltonian, and we see that this works well for depth variation with one and two fast spatial scales.

We also examine peakons and singularity formation in the bidirectional nonlocal system. Peakon initial conditions are generally smoothed and evolve to smooth solitary waves that leave behind radiating tails. However, there is also evidence of cases where the solitary wave is well approximated by a peakon away from its maximum, and may be approaching a peakon as we vary the initial amplitude towards an apparent threshold. Beyond such a threshold we see evidence of blow-up. In the case of profiles with approximate spatial reflection symmetry, the blow-up is preceded by the evolution to a less symmetric profile. The results on peakons are also compared to the ones obtained for unidirectional propagation equations of Whitham type with kernels describing exact and approximate dispersion relations.

2. Mathematical formulation

We consider an ideal fluid, *i.e.* incompressible, irrotational and inviscid, that occupies a time dependent domain $\mathfrak{D}_t$, given by

$$\mathfrak{D}_t(\beta, \eta) := \{(x, y) : x \in \mathbb{R}, -h + \beta(x) < y < \eta(x, t)\},$$

and we assume that $\beta(x) < h$ for all x in $\mathbb{R}$, where h represents the constant reference depth. The mean water level is located at $y = 0$. The lower boundary $-h + \beta(x)$ represents the bottom of the fluid, while $\eta(x, t)$ defines the free surface assumed to be a graph; see Fig. 1.

The equations of motion for the potential flow take the form

$$\partial_t \eta = \partial_y \varphi - (\partial_x \eta)(\partial_x \varphi), \quad \text{on } y = \eta(x, t), \tag{1}$$

$$\partial_t \varphi = -\frac{1}{2}|\nabla \varphi|^2 - g\eta, \quad \text{on } y = \eta(x, t), \tag{2}$$

$$\Delta \varphi(x, y) = 0, \quad \text{on } \mathfrak{D}_t(\beta, \eta), \tag{3}$$

$$\nabla \varphi \cdot N(\beta) = 0, \quad \text{on } y = -h + \beta(x), \tag{4}$$

where $N(\beta) = (1 + (\partial_x \beta)^2)^{-1/2}(\partial_x \beta, -1)$ is the exterior unit normal vector. We are interested in the initial value problem with initial conditions $\eta_0(x)$ and $\varphi_0(x)$ that tend to zero when $x \to \pm\infty$. Defining the function $\xi(x, t) := \varphi(x, \eta(x, t), t)$, the evaluation of the potential at the free surface at time t, we note that we should be able to determine the evolution of φ by the evolution of η and ξ. To formulate (1)–(4) as an evolution equation for η, and ξ, define the Dirichlet–Neumann operator G by

$$(G(\beta, \eta)\xi)(x) = (1 + (\partial_x \eta(x))^2)^{1/2} \nabla \varphi(x, \eta(x)) \cdot N(\eta(x)),$$

where $N(\eta(x)) = (1 + (\partial_x \eta(x))^2)^{-1/2}(-\partial_x \eta(x), 1)$, $x \in R$, and φ is the solution of

$$\left.\begin{aligned}
\Delta\varphi(x, y) &= 0 && \text{for } (x, y) \text{ in } \mathfrak{D}, \\
\varphi(x, \eta(x)) &= \xi(x) && \text{for } x \text{ in } \mathbb{R}, \\
\frac{\partial\varphi}{\partial\hat{n}}(x, -h + \beta(x)) &= 0 && \text{for } x \text{ in } \mathbb{R},
\end{aligned}\right\} \tag{5}$$

where $\hat{n}$ denotes the exterior normal derivative on $\partial\mathfrak{D}$.

It is shown in [9], that the water wave problem (1)–(4) is formulated as the evolution equation for ξ and η in the form

$$\eta_t = G(\beta, \eta)\xi, \tag{6}$$

$$\xi_t = -\frac{1}{2(1 + \eta_x^2)}\left(\xi_x^2 - (G(\beta, \eta)\xi)^2 + 2\eta_x \xi_x G(\beta, \eta)\xi\right) - g\eta. \tag{7}$$

The total energy of the system of the equations for fluid motion is denoted by H, which is the sum of the kinetic energy K, and potential energy U:

$$\begin{aligned}
H &= K + U \\
&= \int_{\mathbb{R}} \int_{-h+\beta(x)}^{\eta(x)} \frac{1}{2}|u|^2 \mathrm{d}y\mathrm{d}x + \int_{\mathbb{R}} \int_{-h+\beta(x)}^{\eta(x)} gy\, \mathrm{d}y\, \mathrm{d}x \\
&= \int_{\mathbb{R}} \int_{-h+\beta(x)}^{\eta(x)} \frac{1}{2}|\nabla\varphi|^2\, \mathrm{d}y\, \mathrm{d}x + \int_{\mathbb{R}} \frac{1}{2}g\eta^2\, \mathrm{d}x - C_\beta,
\end{aligned} \tag{8}$$

where the constant C_β is irrelevant to the dynamics and can be omitted. It is shown in [10], that the water wave equations are Hamiltonian in the form

$$\partial_t \begin{pmatrix} \eta \\ \xi \end{pmatrix} = \begin{pmatrix} 0 & \mathbb{I} \\ -\mathbb{I} & 0 \end{pmatrix} \begin{pmatrix} \dfrac{\delta H}{\delta \eta} \\ \dfrac{\delta H}{\delta \xi} \end{pmatrix}, \tag{9}$$

where H is given by (8) with $C_\beta = 0$.

The Hamiltonian (8) can be expressed through the Dirichlet–Neumann operator, and takes the form

$$H = \frac{1}{2}\int_{\mathbb{R}} \left(\xi G(\beta, \eta)\xi + g\eta^2\right)\mathrm{d}x. \tag{10}$$

We now use the expansion of G in powers of η developed by Craig et al. [7] to obtain shallow water equations for variable depth. Following Craig and Groves [11], we use the approximate expressions for G in the Hamiltonian (10) to derive shallow water models that are also Hamiltonian. In particular, the Dirichlet–Neumann operator is expanded in the amplitude of the free surface in the form

$$G(\beta, \eta) = G_0(\beta, \eta) + G_1(\beta, \eta) + G_2(\beta, \eta) + \cdots, \tag{11}$$

where G_k is homogeneous of degree k in η.

The main result is that the nonlocal operators $G_k(\beta, \eta)$ can be explicitly given for small perturbations of the undisturbed depth h in a recursive form. The first three terms are

$$G_0 = D\tanh(hD) + DL(\beta), \tag{12}$$

$$G_1 = D\eta D - G_0\eta G_0,$$

$$G_2 = \frac{1}{2}\left(G_0 D\eta^2 D - D^2\eta^2 G_0 - 2G_0\eta G_1\right),$$

where $D = -i\partial_x$. The operator $L(\beta)$ in (12) can be written in powers of the depth variation β as $L(\beta) = \sum_{j=1}^{\infty} L_j(\beta)$, with the L_j homogeneous of degree j in β. The first two terms in the expansion of $L(\beta)$ are

$$L_1(\beta) = -\operatorname{sech}(hD)\beta D\operatorname{sech}(hD),$$

$$L_2(\beta) = \operatorname{sech}(hD)\beta D\sinh(hD)L_1(\beta). \tag{13}$$

The zeroth order term G_0 in (12) is the Dirichlet–Neumann operator for a domain with a flat surface $\eta \equiv 0$, and splits into a constant depth part $D\tanh(hD)$ and the part $DL(\beta)$ that contains the bottom topography information.

We thus see that for small amplitude of the waves, and small perturbations of the bottom profile, a truncation of the expansion for the Dirichlet–Neumann operator, gives a nonlocal evolution equation with pseudodifferential operators defined explicitly only on the surface variables. It must be noted that the simplification for β small makes the Hamiltonian explicit.

To introduce the shallow water theory, define the three nondimensional parameters, $\alpha = a/h$, $\delta = (h/l)^2$, and $\gamma = b/h$, where a is the typical amplitude, l is the typical wave-length, h is the average depth, and b is the typical bottom amplitude; see Fig. 1. The dimensionless variables are given by

$$x^* = \frac{x}{l}, \qquad t^* = \frac{t}{l/c_0}, \qquad \eta^* = \frac{\eta}{a}, \qquad \xi^* = \frac{\xi}{gla/c_0}, \quad \text{and} \quad \beta^* = \frac{\beta}{b}. \tag{14}$$

In what follows we drop the * from the dimensionless variables.

From Eq. (10), the approximate Hamiltonian takes the form of a polynomial in η of pseudodifferential operators acting on the variable ξ. To obtain the Boussinesq–Whitham approximation we Taylor expand all Fourier multipliers such as $\tanh(hD)$ in G in powers of the derivative hD. However, to keep the full linear dispersion relation we follow Whitham and use the exact expression for the constant depth quadratic part $\frac{1}{2}\int \xi D \tanh(hD)\xi$ of H, and apply the expansion to powers of derivatives in all the remaining terms of H. Finally, we use the usual Boussinesq scaling to approximate the remaining terms. To this end we scale the wave length in the shallow water form $l = h/\sqrt{\delta}$, and take $\varepsilon := \alpha = \delta = \gamma \ll 1$. We then have $H = H_0 + \mathcal{O}(\epsilon^2)$, with H_0 the "Boussinesq–Whitham" Hamiltonian given by

$$H_0 = \frac{1}{2}\int_{-\infty}^{\infty}\left(\xi\frac{D}{\sqrt{\varepsilon}}\tanh(\sqrt{\varepsilon}D)\xi - \varepsilon\beta(\partial_x\xi)^2 + \varepsilon\eta(\partial_x\xi)^2 + \eta^2\right)dx. \tag{15}$$

Thus in approximating H by H_0 all deleted terms are of $\mathcal{O}(\epsilon^2)$. Hamilton's equation (9) for (15) gives the following system

$$\eta_t = -\partial_x\frac{\tanh(\sqrt{\varepsilon}D)}{\sqrt{\varepsilon}D}u + \varepsilon\partial_x(\beta u) - \varepsilon\partial_x(\eta u), \tag{16}$$

$$u_t = -\partial_x\eta - \frac{\varepsilon}{2}\partial_x(u^2), \tag{17}$$

where we have also introduced the variable $u := \partial_x\xi$. Note that the symbol of the pseudodifferential operator $\tanh(\sqrt{\varepsilon}D)/\sqrt{\varepsilon}D$ is a smooth function, and therefore is well defined; see [12]. The system (16)–(17) can be rewritten as

$$\partial_t\begin{pmatrix}\eta\\u\end{pmatrix} = \begin{pmatrix}0 & -\partial_x\\-\partial_x & 0\end{pmatrix}\begin{pmatrix}\dfrac{\delta H_1}{\delta\eta}\\[2mm]\dfrac{\delta H_1}{\delta u}\end{pmatrix}, \tag{18}$$

where

$$H_1 = \frac{1}{2}\int_{-\infty}^{\infty}\left(u\frac{\tanh(\sqrt{\varepsilon}D)}{\sqrt{\varepsilon}D}u - \varepsilon\beta u^2 + \varepsilon\eta u^2 + \eta^2\right)dx. \tag{19}$$

The cosymplectic operator

$$J = \begin{pmatrix}0 & -\partial_x\\-\partial_x & 0\end{pmatrix}, \tag{20}$$

is seen to be skew-symmetric upon integration by parts, and fulfills the Jacobi identity since it is independent of the dynamical variables.

Finally, note that besides H_1, the mass functional

$$M(\eta) := \int_{-\infty}^{\infty}\eta\,dx, \tag{21}$$

and the linear momentum functional

$$I(u) := \int_{-\infty}^{\infty}u\,dx \tag{22}$$

are conserved quantities of system (16)–(17). The conservation of H_1, M, and I will be used to assess the accuracy of the numerical solutions.

3. Effective equation

To study homogenized equations for rough bottoms we assume that the bottom depends on two scales. Making reference to Fig. 1, we denote by d the typical wavelength of the bottom, and suppose that $\beta := \beta(x, x/d)$ and that it is P-periodic with respect to the second entry. Therefore, the dimensionless bottom β^* is expressed as

$$\beta^* = \frac{\beta(x, x/d)}{b}.$$

We are going to suppose that $d/l = \sqrt{\varepsilon}$. Hence, dropping off the *, the dimensionless bottom is $\beta = \beta(x, x/\sqrt{\varepsilon})$. Then the homogenized equations of motion are obtained averaging the Hamiltonian (19), with respect to the fast variable $x/\sqrt{\varepsilon}$,

$$H_1 = \frac{1}{2} \int_{-\infty}^{\infty} \left(u \frac{\tanh(\sqrt{\varepsilon}D)}{\sqrt{\varepsilon}D} u - \varepsilon \overline{\beta} u^2 + \varepsilon \eta u^2 + \eta^2 \right) dx + \mathcal{O}(\varepsilon^2), \tag{23}$$

where

$$\overline{\beta}(x) = \frac{1}{P} \int_0^P \beta(x, y) dy. \tag{24}$$

Neglecting the terms $\mathcal{O}(\varepsilon^2)$ in (23), we get the effective Hamiltonian, from which we finally obtain the averaged system

$$\eta_t = -\partial_x \frac{\tanh(\sqrt{\varepsilon}D)}{\sqrt{\varepsilon}D} u + \varepsilon \partial_x(\overline{\beta}u) - \varepsilon \partial_x(\eta u), \tag{25}$$

$$u_t = -\partial_x \eta - \frac{1}{2} \varepsilon \partial_x (u^2). \tag{26}$$

where $\overline{\beta}$ depends only on one scale. It is to be noted that the assumption β small avoids solving the cell problem which is a major numerical step.

The idea of homogenizing by using two-scale expansions of integrals in the Hamiltonian appears in [7], where we also find a justification for these expansions.

4. Numerical solution

To solve the system (16)–(17) we use the Fourier collocation method; see [13]. We consider L-periodic boundary conditions in the domain $[-L/2, L/2)$ and choose the N collocation points as $x_j = Lj/N - L/2$, for $j = 0, \ldots, N - 1$. Also, let S_N denote the span of trigonometric polynomials $\{\exp(i(2\pi k/L)x)\}$, with $k \in \mathbb{Z}$, $N/2 \le k \le N/2 - 1$. The functions of interest $(\eta(x), u(x))^\top$ are approximated as

$$\begin{pmatrix} \eta \\ u \end{pmatrix} = \sum_{k=-N/2}^{N/2-1} \begin{pmatrix} \tilde{\eta}_k \\ \tilde{u}_k \end{pmatrix} \exp(i(2\pi k/L)x), \tag{27}$$

where $\tilde{\eta}_k, \tilde{u}_k$ are Fourier interpolation coefficients; see [13] for details. We thus solve the system

$$\frac{d}{dt} \begin{pmatrix} \boldsymbol{\eta} \\ \mathbf{u} \end{pmatrix} = \begin{pmatrix} \mathbf{f}_1(\boldsymbol{\eta}, \mathbf{u}) \\ \mathbf{f}_2(\boldsymbol{\eta}, \mathbf{u}) \end{pmatrix} \tag{28}$$

where

$$\mathbf{f}_1(\boldsymbol{\eta}, \mathbf{u}) = -\mathcal{F}^{-1}\{i \tanh(\mathbf{k}) \boxtimes \mathcal{F}(\mathbf{u})\} + \mathcal{F}^{-1}\{i\mathbf{k} \boxtimes \operatorname{sech}(\mathbf{k}) \boxtimes \mathcal{F}\{\boldsymbol{\beta} \boxtimes \mathcal{F}^{-1}(\operatorname{sech}(\mathbf{k}) \boxtimes \mathcal{F}(\mathbf{u}))\}\} \\ - \mathcal{F}^{-1}\{i\mathbf{k} \boxtimes \mathcal{F}\{\mathbf{u} \boxtimes \boldsymbol{\eta}\}\}, \tag{29}$$

$$\mathbf{f}_2(\boldsymbol{\eta}, \mathbf{u}) = -\mathcal{F}^{-1}(i\mathbf{k} \boxtimes \mathcal{F}(\boldsymbol{\eta})) - \frac{1}{2}\mathcal{F}^{-1}\{i\mathbf{k} \boxtimes \mathcal{F}(\mathbf{u} \boxtimes \mathbf{u})\}, \tag{30}$$

where $\mathcal{F}, \mathcal{F}^{-1}$ denote the discrete Fourier and inverse Fourier transforms respectively, $\mathbf{a} \boxtimes \mathbf{b}$ denotes component-wise multiplication of vectors $\mathbf{a}, \mathbf{b}$ in $\mathbb{C}^N$, and

$$\mathbf{k} = (-N/2, -N/2 + 1, \ldots, N/2 - 1)^\top,$$
$$\mathbf{u} = (u_0, u_1, \ldots, u_{N-1})^\top,$$
$$\boldsymbol{\eta} = (\eta_0, \eta_1, \ldots, \eta_{N-1})^\top,$$
$$\boldsymbol{\beta} = (\beta(x_0), \beta(x_1), \ldots, \beta(x_{N-1}))^\top,$$

for $-N/2 \le k \le N/2 - 1$. The initial conditions are

$$\boldsymbol{\eta}(0) = (\eta(x_0), \eta(x_1), \ldots, \eta(x_{N-1}))^\top,$$
$$\mathbf{u}(0) = (u(x_0), u(x_1), \ldots, u(x_{N-1}))^\top.$$

The number of collocation points that we use is a power of 2. Therefore, while the initial conditions are real functions, their trigonometric interpolates can be complex. To avoid this we set $\tilde{\eta}_{-N/2}$ and $\tilde{u}_{-N/2}$ in (27) equal to zero; see [13, p. 123].

To integrate numerically system (28), we use a fourth-order Adams–Bashford/Moulton (ABM) predictor–corrector scheme (see [14,15, Section III.1]). The ABM predictor/corrector scheme requires two functional evaluations per step. It is therefore faster than the fourth order Runge–Kutta and has less error accumulation per step. The method was initiated
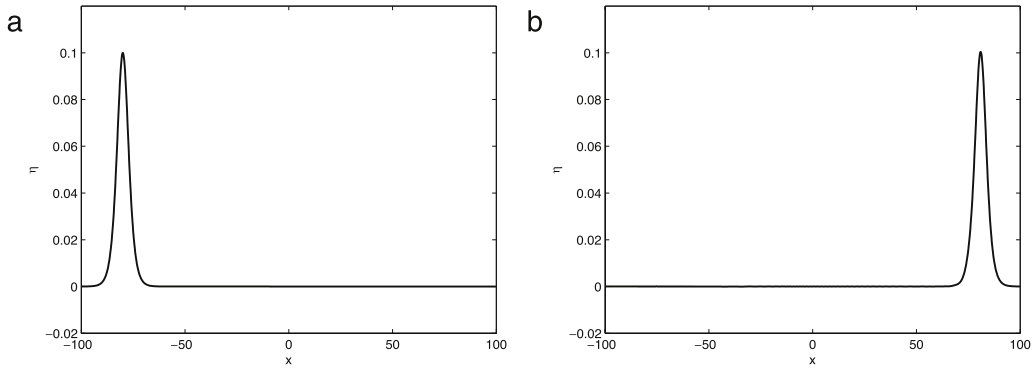
Fig. 2. (a) The initial wave profile. (b) A soliton moving to the right at time $t = 160.103$.

with a fourth-order Runge–Kutta scheme. We may also expect that any possible high frequencies that could arise while solving our equation can be resolved by the ABM predictor/corrector. Accordingly, the predictor is defined as

$$y_{n+1} = y_n + \frac{\Delta t}{24}(55\dot{y}_n - 59\dot{y}_{n-1} + 37\dot{y}_{n-2} - 9\dot{y}_{n-3}),$$

and the corrector as

$$y_{n+1} = y_n + \frac{\Delta t}{720}(251\dot{y}_{n+1} + 646\dot{y}_n - 264\dot{y}_{n-1} + 106\dot{y}_{n-2} - 19\dot{y}_{n-3}).$$

For all the numerical experiments that we show we considered smooth initial conditions η and u with rapid decay as $x \to \pm\infty$, so that we can consider $u(-L/2) = u(L/2)$ and $\eta(-L/2) = \eta(L/2)$ up to a small error. We choose the time step Δt and the spatial step Δx, in such a way that the relative error of the conserved quantities (19), (21) and (22) is typically around 10^{-14}. This ascertains the accuracy of our numerical solution. The numerical scheme was implemented in MATLAB.

In addition, given η we took u in such a way that it satisfies the first order terms of the linear part of (16)–(17), *i.e.* $\eta_t = -u_x$ and $u_t = -\eta_x$. This approximation is appropriate since it gives a good description of the motion of surface water waves on a short time and it is used to put as initial conditions exact solutions of unidirectional equations that involve only η.

5. Solitary wave solutions for constant depth

It is well known that unidirectional shallow water wave equations such as the KdV, the Camassa–Holm, and the BBM (see [16]) have localized traveling wave solutions. In the case of the KdV and Camassa–Holm equations these traveling waves, known as solitons (and peakons in some cases of the Camassa–Holm equation), have elastic collisions with phase-shift. We want to determine whether system (16)–(17) with a flat bottom also has solitons. To the best of our knowledge there has not been previous research on such a bidirectional equation with the full dispersion relation of linear waves. Ehrnström et al. [17] have recently proved the existence of solitons for a Whitham equation with the full linear dispersion, see also chapter 8, and Eq. (42) with kernel (43).

To study the evolution of KdV-type (*i.e.* unidirectional) initial conditions in the system (16)–(17), we use $L = 200$, $\varepsilon = 0.1$, and $N = 1024$, and the initial condition

$$\eta_0 = u_0 = 0.1\text{sech}^2(0.27(x + 80)). \tag{31}$$

The initial value satisfies the amplitude/width ratio of the KdV soliton traveling to the right, as shown in Fig. 2(b). The equations were integrated up to a time $t = 165$. In Fig. 2(b), we show the evolution of this initial condition into a more permanent form with no radiation shed (to graphical accuracy).

We now consider the evolution of the following initial condition

$$\eta_1(x) = u_1(x) = 0.3\,\text{sech}^2(0.7\,(x + 780)). \tag{32}$$

The amplitude has the functional form of a KdV soliton but the amplitude/width ratio is different from that of the KdV soliton. The length of the channel is $L = 1600$, the number of nodes $N = 8192$, and $\varepsilon = 0.3$. As in the KdV approximation the initial condition sheds radiation, see Fig. 3(a), and a peak detaches and travels, as shown in Fig. 3(b), as a solitary wave. Zooming into Fig. 3(a) and (b), we see that the traveling waves shown there are smooth.

The KdV soliton solutions have the characteristic property that their collision is elastic, with a small phase-shift. We see numerical evidence that similar phenomena occur in system (16)–(17) as well. To study the interaction we consider the overtaking of a small KdV soliton by a larger one. We take $\varepsilon = 0.3$, $\beta \equiv 0$, $L = 1800$, and $N = 4096$. The initial condition

$$\eta_2(x) = u_2(x) = 0.3\,\text{sech}^2(0.55\,(x + 880)) + 0.1\,\text{sech}^2(0.32\,(x + 850)), \tag{33}$$

is shown in Fig. 4(a)
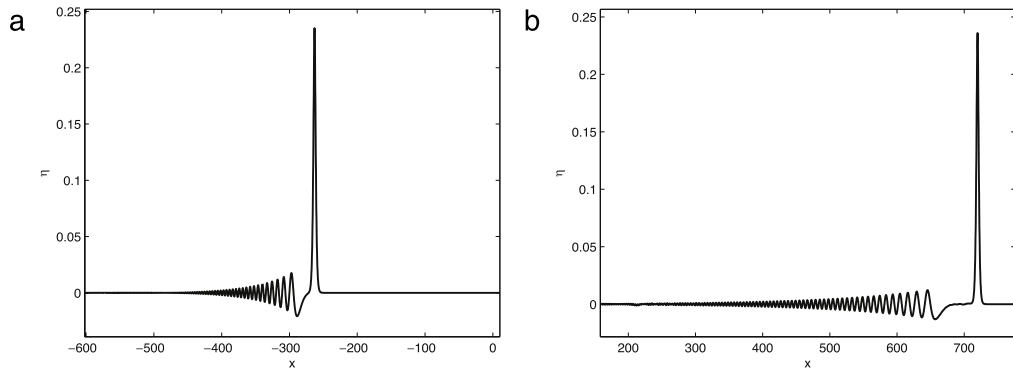
Fig. 3. (a) The evolution of the initial condition (32), at time $t = 500.103$. (b) The evolution at time $t = 1450.106$.
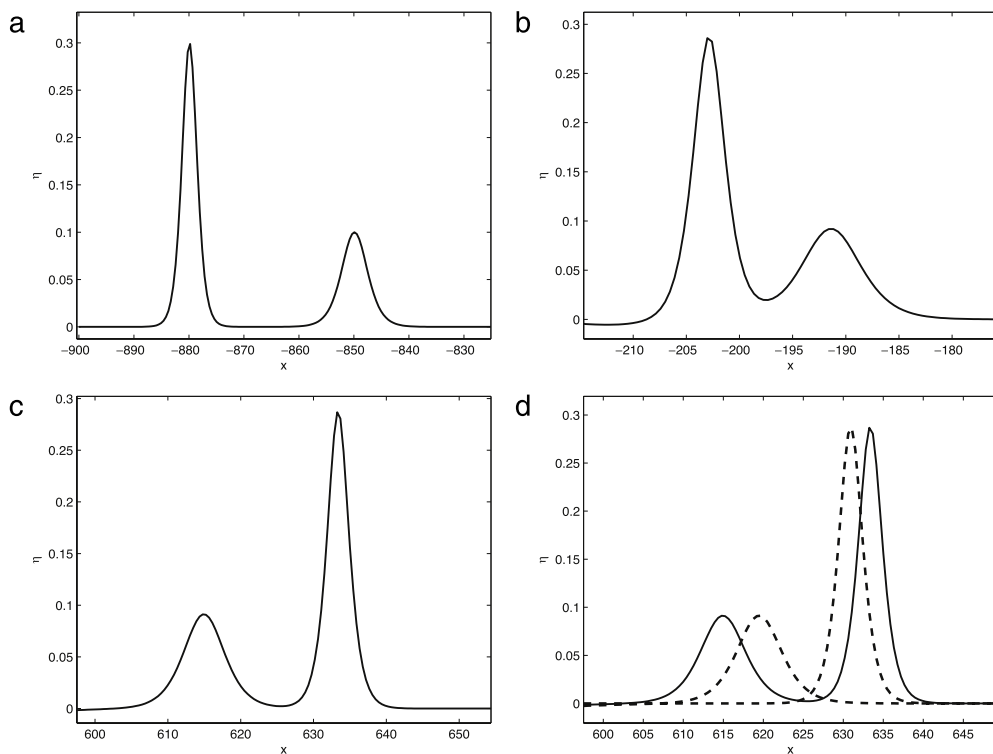
Fig. 4. (a) Initial condition. (b) Solitons moving to the right at time $t = 650.103$, before the overtaking. (c) Solitons moving to the right at time $t = 1450.103$, after the overtaking. (d) A comparison of the solitons that evolved without any interaction (dashed lines) and the ones that interacted (solid line) at time $t = 1450.103$.

In Fig. 4(b)–(c), we show two stages of the evolution and observe that the solitons shed little radiation in the process. In Fig. 4(d), dashed lines represent the evolution from each of the two terms in (33). This demonstrates a clean interaction with a phase-shift that is qualitatively similar to the one seen in the KdV, *i.e.* in the exact soliton solution. It must be remarked that the chosen two soliton initial condition is not an exact solution for the KdV. However, this experiment helps us to give a qualitative description of the interaction of two soliton-type waves with different amplitudes.

Note that despite the qualitative agreement with KdV behavior, we also observe some differences. For example the KdV soliton initial condition (31) we used disperses to zero when its amplitude is sufficiently small. This is unlike the KdV were a similar initial condition of arbitrarily small amplitude still propagates as a soliton.

Finally, we consider the head-on collision of two KdV-type solitary waves. For this, we take the following initial condition

$$\begin{cases} \eta_3(x) = 0.3 \operatorname{sech}^2(0.27 \, (x + 85)) + 0.3 \operatorname{sech}^2(0.27 \, (x - 85)), \\ u_3(x) = 0.3 \operatorname{sech}^2(0.27 \, (x + 85)) - 0.3 \operatorname{sech}^2(0.27 \, (x - 85)). \end{cases} \tag{34}$$
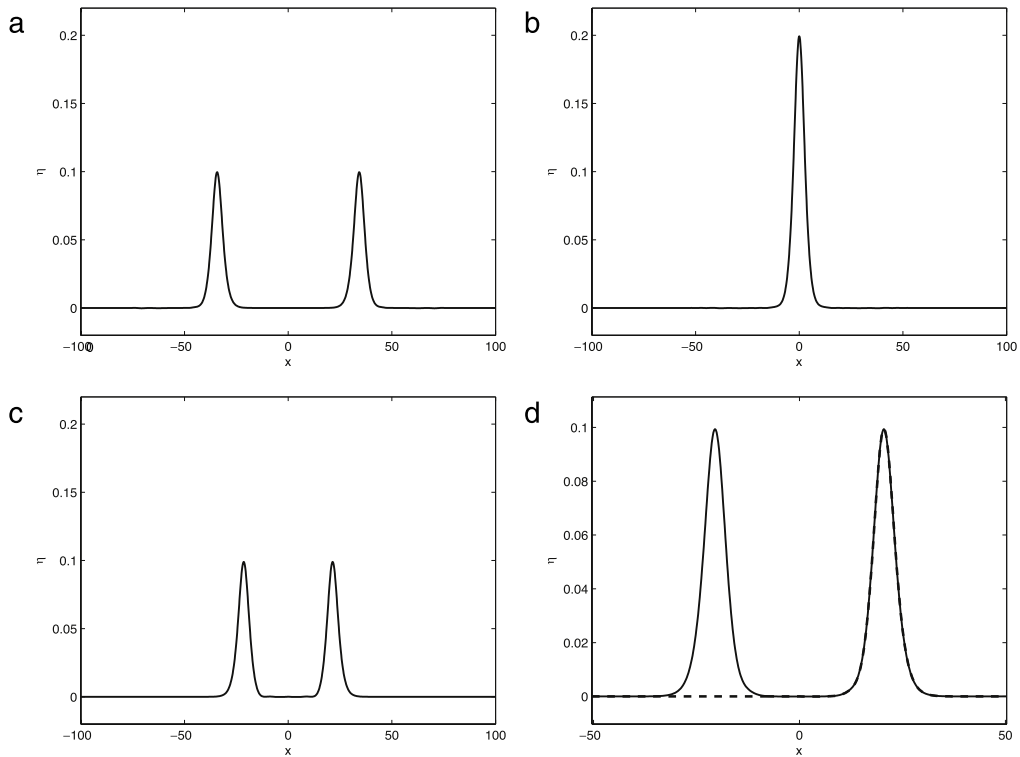
Fig. 5. (a) Two solitons at time $t = 50.103$, moving with the same speed in opposite directions, towards each other. (b) Solitons at time $t = 84.103$ during the collision. (c) The solitons have emerged, and move in opposite direction away from each other. Snapshot at time $t = 105.103$. (d) Comparison of solitons that collided (solid line) and the single soliton (dashed line) corresponding to the left peak of Fig. 5(a). Snapshot at time $t = 105.103$. If we zoom we see a very small phase-shift.

The solitons start moving towards each other shedding negligible radiation; see Fig. 5(a). In Fig. 5(b) we show a moment of the collision, and in Fig. 5(c) they have emerged unchanged. In Fig. 5(d) we show in dashed lines the shapes of the single solitons.

6. Solitary wave evolution over smooth depth topography

We have provided numerical evidence that system (16)–(17) has solitary wave solutions. We now examine what happens to solitary waves as they go through a slope. We generally see the reflection of a small amplitude wave.

To see a typical situation we use $\varepsilon = 0.35$, $L = 200$, and $N = 1024$. The bottom shape is given by the single space scale function

$$\beta(x) = \begin{cases} 0, & \text{if } -100 \leq x \leq -49, \\ \dfrac{0.3}{2}\big(1 - \cos(0.2(x - 49))\big), & \text{if } -49 < x \leq -33.5, \\ 0.3, & \text{if } -33.5 \leq x \leq 33.5, \\ \dfrac{0.3}{2}\big(1 - \cos(0.2(x - 18.5))\big), & \text{if } 33.5 \leq x \leq 49, \\ 0, & \text{if } 49 \leq x \leq 100, \end{cases} \tag{35}$$

and the initial condition is

$$\eta(x) = u(x) = 0.1 \operatorname{sech}^2(0.27(x + 80)). \tag{36}$$

In Fig. 6(b) we can appreciate a small wave that is propagating to the left with a negligible change in its shape. This wave was created as the result of the interaction between the wave that goes to the right and the bottom, albeit, it cannot be seen in Fig. 6(a) due to the scales of the plot. This result is consistent with the asymptotic results of Smyth [18].

7. Evolution of solitary waves above a rough bottom topography

It is well established that linear waves are more affected by a rapid depth variations than slowly varying, smooth bottom topographies. We now examine the effect of rapid depth variations on solitons of (weakly nonlinear) shallow water wave theories, in particular we want to examine the validity of the homogenization approximations proposed by Craig et al. [7].
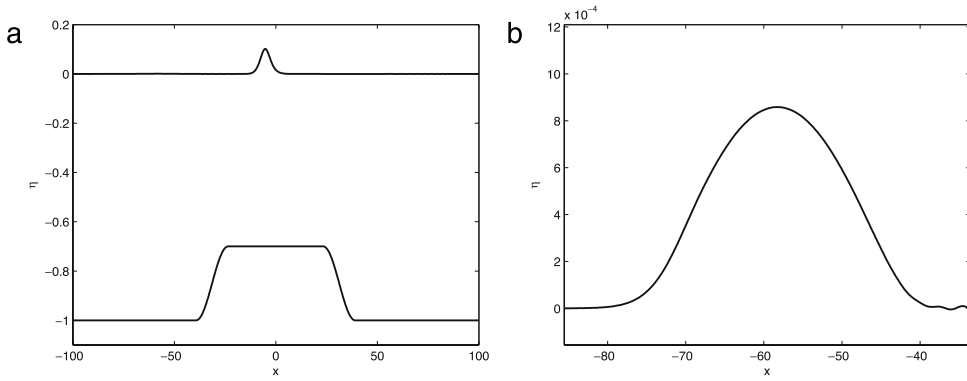
Fig. 6. (a) Soliton-type wave at time $t = 75.103$, moving to the right. (b) A zoom of Fig. 6(a) is shown.
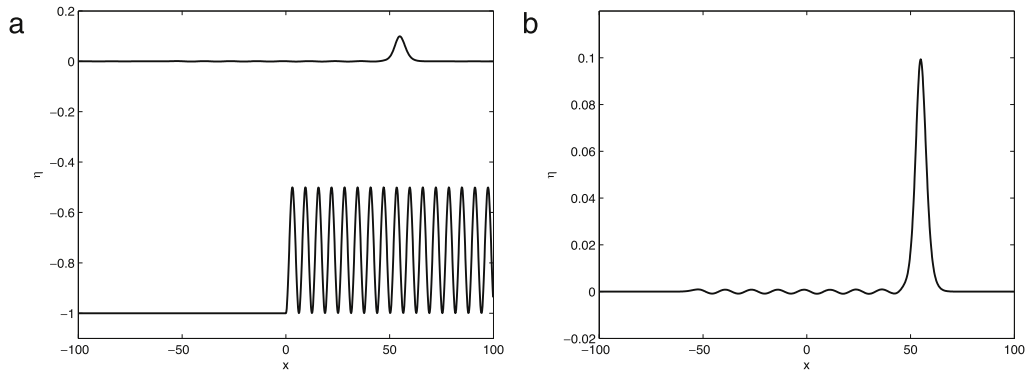
Fig. 7. (a) The numerical solution of (16)–(17) with initial conditions (37) at time $t = 125.103$. (b) A zoom near the wave of highest amplitude of Fig. 7(a).

In all the numerical results of this section we use $\varepsilon = 0.1$, $N = 1024$, $\Delta t = 0.001$, and the length of the channel is $L = 200$. The initial condition is a KdV-type soliton

$$\begin{cases} \eta_0(x) = 0.1 \operatorname{sech}^2(0.27(x + 80)), \\ u_0(x) = 0.1 \operatorname{sech}^2(0.27(x + 80)). \end{cases} \tag{37}$$

For the first experiment we take the bottom in the form

$$\beta(x) = \begin{cases} 0, & \text{if } -100 \leq x \leq 0, \\ \dfrac{0.5}{2}(1 - \cos(x)), & \text{if } 0 < x \leq 100. \end{cases} \tag{38}$$

The evolution is shown in Fig. 7(a), and a zoom is shown in Fig. 7(b).

These figures show how the soliton evolves shedding backwards a reflected wave. The theory of Section 3, gives an effective equation with a constant effective depth variation of

$$\overline{\beta} = \frac{1}{2\pi} \int_0^{2\pi} \frac{0.5}{2}(1 - \cos(x)) \mathrm{d}x = 0.25, \tag{39}$$

i.e. comparing to (24), here $\cos(x)$ represents a fast scale ($\overline{\beta}$ does not have a slow scale and is constant). (39) gives an effective velocity $\overline{c} = \sqrt{1 - 0.25\varepsilon}$ for the long waves of the linear part of (25)–(26). This speed is smaller than the constant depth speed for long waves. In fact, this correction to the linear speed predicts accurately the phase-shift seen in Fig. 8(a) and (b).

Finally, in Fig. 9(a) and (b), we present the comparison between the numerical solution with the rough bottom (38), and the numerical solution with the homogenized bottom (39). The comparison shows a remarkable correction of the phase-shift.

Now we will consider the case in which the bottom depends on two scales. Let us consider the following bottom profile

$$\beta(x, 5x) = \begin{cases} 0, & \text{if } -100 \leq x \leq 0, \\ \dfrac{0.5}{2}\Big(1 - \cos(x)\cos^2(5x)\Big), & \text{if } 0 < x \leq 100. \end{cases} \tag{40}$$
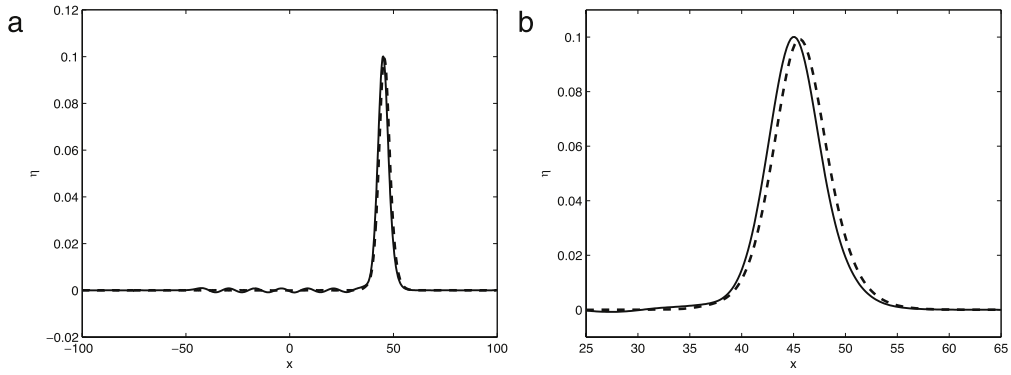
Fig. 8. (a) Comparison between the numerical solution of (16)–(17) with initial conditions (37) at time $t = 125.103$. The solid line corresponds to the bottom (38) and the dashed line to a flat bottom. (b) A zoom near the wave of highest amplitude of Fig. 8(a) shows a phase-shift of the solutions.
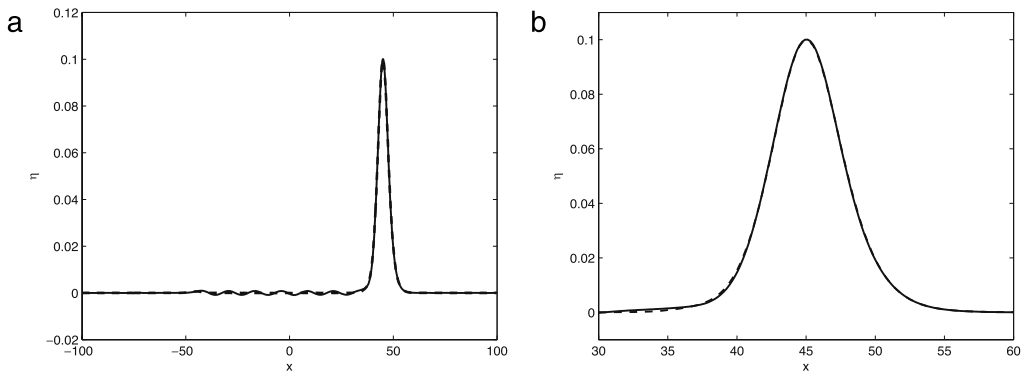
Fig. 9. (a) Comparison between the numerical solution of (16)–(17) with initial conditions (37) at time $t = 125.103$. The solid line corresponds to the bottom (38) and the dashed line to (39). (b) A zoom near the wave of highest amplitude of Fig. 9(a) shows a negligible phase-shift.
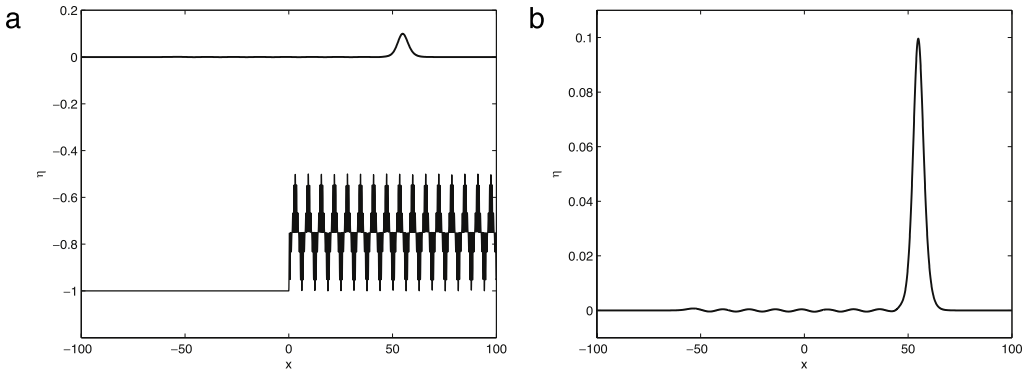
Fig. 10. (a) Numerical solution of the system (16)–(17) with initial condition (37), and bottom (40) at time $t = 125.103$. (b) A zoom near the wave of highest amplitude of Fig. 10(a).

In Fig. 10(a) we display the evolution of the soliton and in Fig. 10(b) a zoom. As before, there are reflected waves traveling to the left caused by the rough bottom. Again, the homogenization results provide the effective equation upon averaging on the fast spatial scale. The homogenized bottom profile takes the form

$$\overline{\beta}(x) = \frac{0.5}{2} \left(1 - \frac{1}{2} \cos(x) \right). \tag{41}$$

Finally, in Fig. 11(a) we display a comparison between the numerical solution with the rough bottom (40) and the one with a flat bottom. On the other hand, in Fig. 12(a) and Fig. 12(b), we present the comparison between the numerical
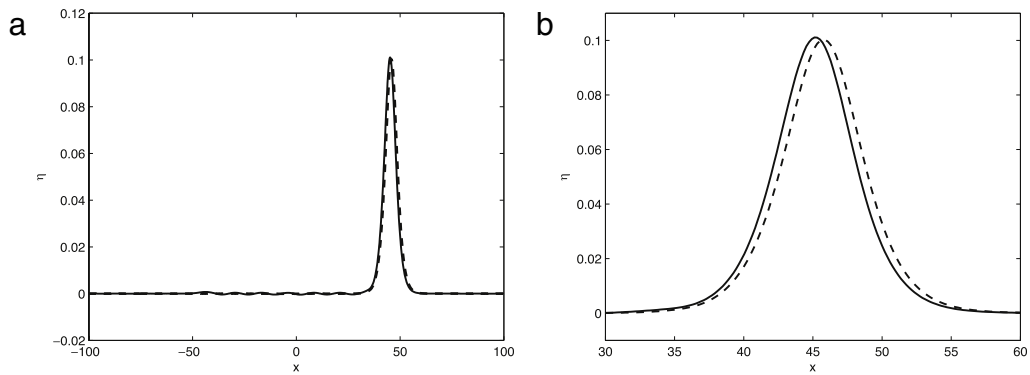
Fig. 11. (a) Comparison between the numerical solution of (16)–(17) with initial conditions (37) at time $t = 125.103$. The solid line corresponds to the bottom (40) and the dashed line to a flat bottom. (b) A zoom near the wave of highest amplitude of Fig. 11(b) shows a phase-shift.
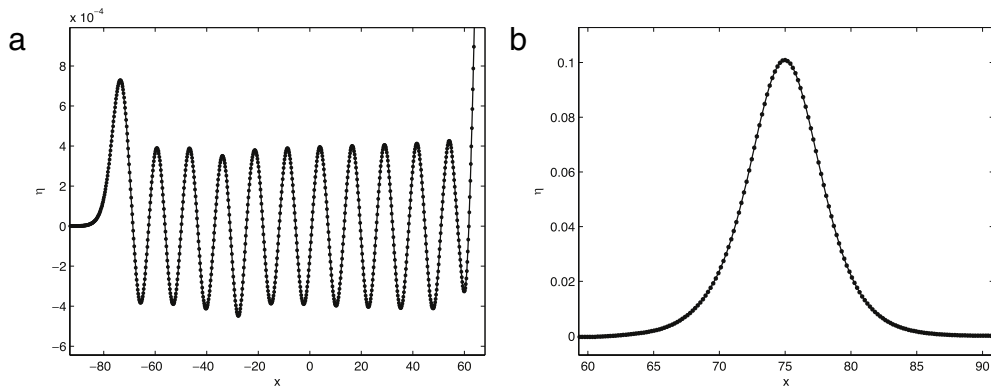
Fig. 12. (a) Comparison between the numerical solution of (16)–(17) with initial conditions (37) at time $t = 155.103$. The solid line corresponds to the bottom (40), and the dashed line the homogenized bottom (41). (b) A zoom near the waves of highest amplitude at time $t = 155.103$, shows a good fitting of the two curves.

solution with the rough bottom (40), and the numerical solution with the homogenized bottom (41). In Fig. 12(a), we show a comparison of the tails and in Fig. 12(b) we display a comparison of the waves of highest amplitude. The comparison is remarkable.

8. Singularity formation and smoothing

The KdV equation does not feature wave breaking, nor peaking, since the initial value problem is globally well-posed in $H^2(\mathbb{R})$ [19]. To capture such phenomena in shallow water wave theory, Whitham [1] suggested equations of the form

$$\begin{cases} \eta_t + \frac{3}{2}\eta\eta_x + \int_{-\infty}^{\infty} K(x - \xi)\eta_\xi(t, \xi)\,\mathrm{d}\xi = 0, \\ \eta(0, x) = \eta_0(x), \end{cases} \tag{42}$$

with kernels that provide better approximations to the exact linear dispersion relation. An example is the singular kernel

$$K_{SW}(x) = \frac{1}{2\pi}\int_{-\infty}^{\infty}\left(\frac{\tanh(\xi)}{\xi}\right)^{1/2} e^{i\xi x}\,\mathrm{d}\xi, \tag{43}$$

which leads to an exact dispersion relation for the linearized water wave equation with constant depth.

Since the kernel (43) is singular, Whitham [1] proposed to study Eq. (42) with the kernel

$$K_P(x) = \frac{\pi}{4}\exp\left(-\frac{\pi}{2}|x|\right), \tag{44}$$

and found the peakon-type traveling wave solution

$$\eta(x, t) = \frac{8}{9}\exp\left(-\frac{\pi}{4}\left|x - \frac{4}{3}t\right|\right). \tag{45}$$
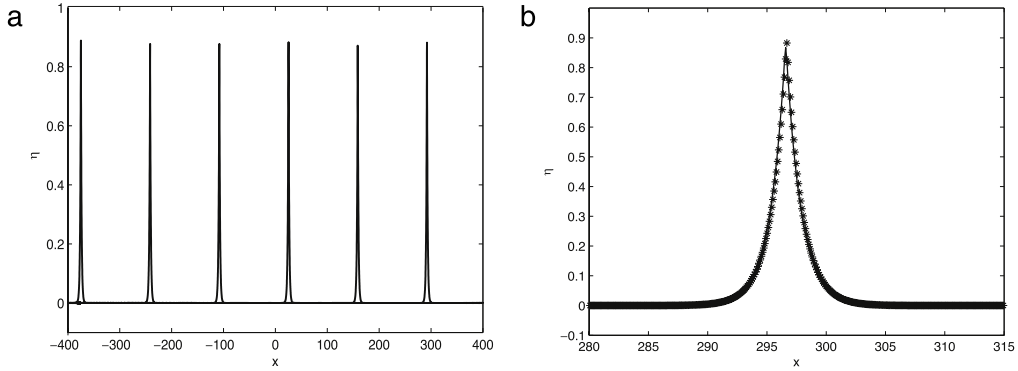
Fig. 13. (a) We display snapshots of the evolution of the initial condition (47) under the Whitham equation (42) with kernel (44), at times (from left to right) 0, 100.003, 200.003, 300.003, 400.003, and 500.003. (b) Comparison between the numerical solution (stars), and the exact solution (45), (solid line).
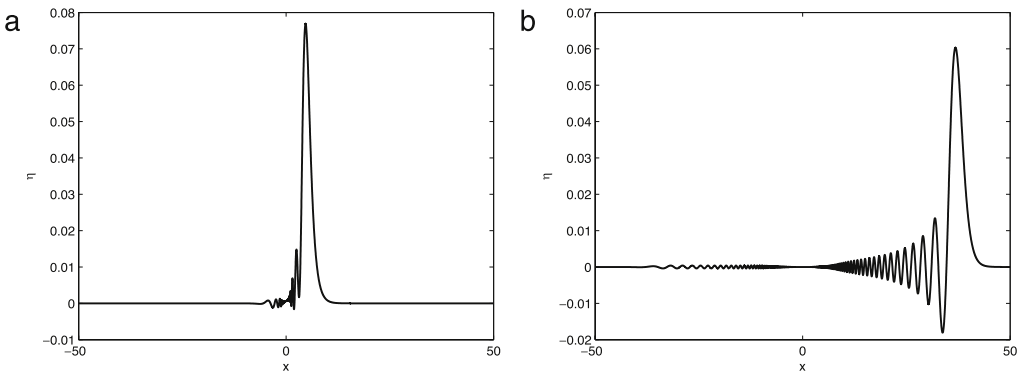
Fig. 14. (a) The evolution of the peakon at time $t = 5.0515$. (b) The evolution at time $t = 37.5515$.

Another equation that exhibits peaked solutions is the Camassa–Holm equation,

$$\eta_t + 2\kappa \eta_x - \eta_{xxt} + 3\eta \eta_x = 2\eta_x \eta_{xx} + \eta \eta_{xxx}, \tag{46}$$

which is completely integrable, and has peaked solutions that interact cleanly when $\kappa = 0$, [20]. Moreover, initial conditions close to a peakon evolve into a leading peakon followed by a tail of radiation formed by peakons of smaller amplitude; see [21]. Constantin and Strauss [25] proved that peakon solutions of the Camassa–Holm equation are stable. However, the stability of such solutions of the Whitham equation with kernel (44) is not known. Also it is not known whether the unidirectional equation (42) with the full dispersion relation (43) has peakon solutions. In this section we study numerically these questions using unidirectional and bidirectional models.

First we give numerical evidence for the stability of peaked solutions of the Whitham equation (42) with the kernel (44). We use $N = 8192$, $L = 800$, and the exact peakon initial condition

$$\eta_0(x) = \frac{8}{9} \exp\left(-\frac{\pi}{4}|x|\right). \tag{47}$$

In Fig. 13(a) we see several snapshots of the evolution of the peakon, and in Fig. 13(b) we show the last frame with the exact solution (45) superimposed. We see that the shape of the peakon does not change as it travels and consider this to be evidence of its stability.

To examine the effect of backward propagating waves we also consider bidirectional model (16)–(17) with peaked initial conditions. We use $\varepsilon = 0.1$, $N = 8192$, $\Delta t = 0.0005$, $L = 100$, and we take $\beta \equiv 0$. The initial condition is

$$\eta_0(x) = u_0(x) = 0.1 \exp(-|x|). \tag{48}$$

The evolution of the relative error of the conserved quantities (19), (21) and (22) is around 10^{-15}. The peaked initial condition is smoothed and moves to the right, leaving behind it a small wave-train, as can be seen in Fig. 14(a) and (b). We observed similar behavior for other peaked initial conditions of small amplitude.

We also examine the behavior of larger amplitude initial conditions for the model (16)–(17) using $N = 9000$, $L = 800$, $\varepsilon = 0.4$, $\Delta t = 0.001$, and $\beta \equiv 0$. The initial condition is

$$\eta_0(x) = u_0(x) = A \operatorname{sech}^2(0.5x). \tag{49}$$
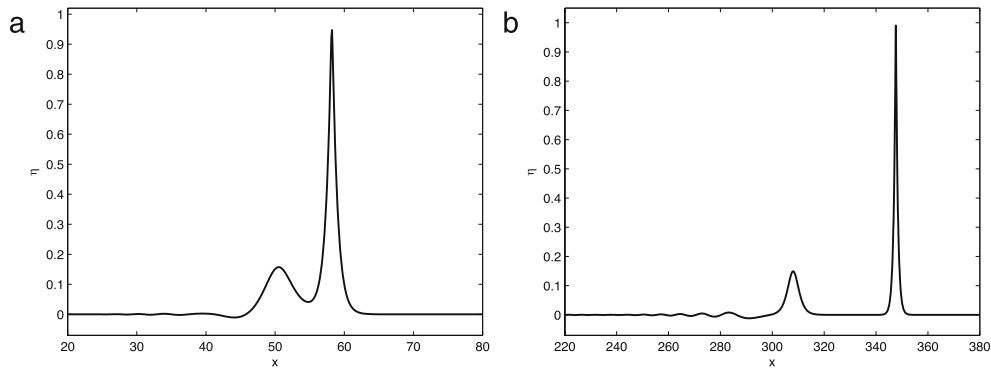
Fig. 15. (a) A zoom near the wave of maximum amplitude at time $t = 50.103$. (b) A zoom of the traveling wave that has emerged is shown at time $t = 300.103$.
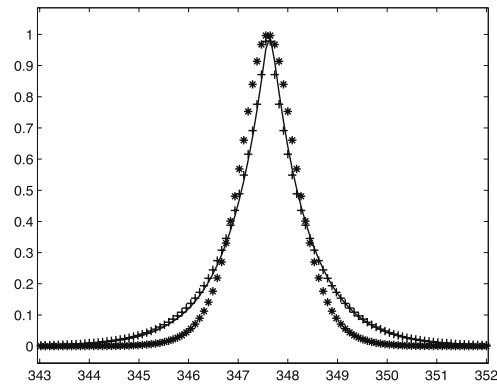
Fig. 16. We display the comparison between the traveling wave shown in Fig. 15(b) (solid line), the fitted peakon curve (crosses) and the fitted KdV soliton curve (stars).

Choosing $A = 0.01$ we see that the profile decays dispersively, without forming a traveling wave. For larger A we see the formation of a traveling wave, that is, a wave form that propagates without changing its shape, leaving behind it a decaying dispersive tail. At $A = 0.58$ it appears that the traveling wave develops a cusp, and at $A = 0.59$ we see evidence of blow up. This behavior is consistent with the results of McLean et al. [22], where traveling waves also appear to have a nonsmooth limiting profile.

In Fig. 15(a) we show the wave of maximum amplitude for $A = 0.58$. We can see how a traveling wave starts to emerge, and in Fig. 15(b) the wave has moved away from the wave-train completely, and travels for a long distance without changing its shape. Since we are interested in the shape of the traveling wave of system (16)–(17) with the initial condition (49), we try to fit the profile with KdV-soliton and peakon shapes, of the form $A\,\mathrm{sech}^2(Bx)$, and $A\exp(-\lambda|x|)$ respectively.

As indicated in Fig. 16, obtained using standard curve fitting tools from MATLAB, the peakon gives a better fit, especially away from the maximum, *e.g.* the sup norm distance for the best fit is 0.0369 for the peakon, and 0.0845 for the KdV soliton. This suggests the possibility of a limiting peaked traveling wave for system (16)–(17). The nature of the cusp however is not resolved in the present study.

Finally, longer amplitude initial conditions lead to breaking. In fact, in the unidirectional model, Seliger [23] showed formally that a sufficiently asymmetric initial profile would break in the typical hyperbolic manner. Recently Constantin and Escher [24] have given a rigorous proof of this result. We now show how the system (16)–(17), exhibits the same behavior even for symmetric initial conditions. To this end, we use $\varepsilon = 0.5, L = 100, N = 1024$, a flat bottom, $\Delta t = 0.001$, and the initial condition

$$\eta_0(x) = u_0(x) = 0.7\,\mathrm{sech}^2(0.5\,x). \tag{50}$$

In Fig. 17, we display the evolution which shows the asymmetry in the early stages followed by the infinite slope of the solution indicating breaking.

9. Conclusions

We have studied numerically a nonlocal Boussinesq–Whitham model for water wave propagation in channels of variable depth. The function describing the variation of the depth is assumed to have small amplitude, but is not necessarily slowly varying.
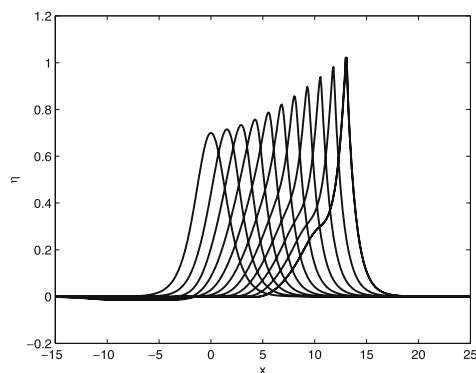
Fig. 17. The evolution of an initial profile until its breaking.

The derivation uses the Hamiltonian formulation of the water wave problem and the expansions of the variable depth Dirichlet–Neumann operator in pseudodifferential operators developed in [7]. To avoid ill-posedness while also keeping some of the simplicity of the shallow water theory we use a model with a nonlocal, exact constant depth dispersion, and local nonlinear and variable depth terms. The resulting system with constant depth captures many known soliton effects and exhibits smoothing and singularity formation.

For variable depth we focus on propagation in oscillatory periodic and two-periodic depth profiles. We see that solitons propagate without any significant deformations, despite the fact that they leave behind an oscillatory tail. Moreover, the propagation of the soliton in the variable depth region can be predicted accurately by an effective constant coefficient Boussinesq–Whitham equation.

Our study has generally considered phenomena where solitons propagate through variable depth regions without significant changes. This seems consistent with the assumption of small amplitude depth variations in the derivation of our model. It would be of interest to understand the phenomena described in this paper theoretically, and examine models where the variation of depth can have more drastic effects.

Acknowledgments

References

[1] G.B. Whitham, Linear and Nonlinear Waves, Wiley, 1974.
[2] R.S. Johnson, On the development of a solitary wave moving over uneven bottom, Proc. Cambridge Philos. Soc. 73 (1973) 183–203.
[3] J.W. Miles, On the Korteweg–de Vries equation for a gradually varying channel, J. Fluid Mech. 91 (1979) 181–190.
[4] T. Iguchi, A long wave approximation for capillary–gravity waves and an effect of the bottom, Comm. Partial Differential Equations 32 (2007) 37–85.
[5] F. Chazel, On the Korteweg–de Vries approximation for uneven bottoms, Eur. J. Mech. B Fluids 28 (2) (2009) 234–252.
[6] R. Rosales, G. Papanicolaou, Gravity waves in a channel with a rough bottom, Stud. Appl. Math. 68 (1983) 89–102.
[7] W. Craig, P. Guyenne, D. Nicholls, C. Sulem, Hamiltonian long-waves expansions for water waves over a rough bottom, Phil. Trans. R. Soc. A 461 (2055) (2005) 839–887.
[8] V.E. Zakharov, Weakly nonlinear waves on the surface of an ideal finite depth fluid, Amer. Math. Soc. Transl. 182 (2) (1998) 167–197.
[9] W. Craig, C. Sulem, Numerical simulation of gravity waves, J. Comp. Phys. 108 (1994) 73–83.
[10] V.E. Zakharov, Stability of periodic waves of finite amplitude on the surface of a deep fluid, J. Appl. Mech. Tech. Phys. 9 (1968) 1990–1994.
[11] W. Craig, M. Groves, Hamiltonian long-wave scaling limits of the water-wave problem, Wave Motion 19 (1994) 367–389.
[12] M.E. Taylor, Pseudodifferential Operators, Princeton University Press, 1981.
[13] C.G. Canuto, M.Y. Hussaini, A. Quarteroni, T.A. Zang, Spectral Methods: Fundamentals in Single Domains, in: Scientific Computation, Springer Verlag, 2006.
[14] W.J.D. Bateman, C. Swan, P.H. Taylor, On the efficient numerical simulation of directionally spread surface water waves, J. Comput. Phys. 174 (2001) 277–305.
[15] E. Hairer, S.P. Nørsett, G. Wanner, Solving Ordinary Differential Equations I: Nonstiff Problems, second ed., Springer Verlag, Berlin, 1993.
[16] T.B. Benjamin, J.L. Bona, J.J. Mahony, Model equations for long waves in nonlinear dispersive systems, Phil. Trans. R. Soc. A 272 (1972) 47–78.
[17] M. Ehrnström, M.D. Groves, E. Wahlén, Solitary waves of the Whitham equation—a variational approach to a class of nonlocal evolution equations and existence of solitary waves of the Whitham equation, Preprint, 2012.
[18] N.F. Smyth, I. Soliton on a beach and related problems. II. Modulated capillary waves, Ph.D. Thesis, California Institute of Technology, 1984.
[19] J. Bona, R. Scott, Solutions of the Korteweg–de Vries equation in fractional order Sobolev spaces, Duke Math. J. 43 (1976) 87–99.
[20] R. Camassa, D.D. Holm, An integrable shallow water equation with peaked solitons, Phys. Rev. Lett. 71 (11) (1993) 1661–1664.
[21] R. Camassa, D.D. Holm, J.M. Hyman, A new integrable shallow water equation, Adv. Appl. Mech. 31 (1994) 1–33.
[22] J.W. McLean, Y.C. Ma, D.U. Martin, P.G. Saffman, H.C. Yuen, Three dimensional instability of finite-amplitude water waves, Phys. Rev. Lett. 46 (13) (1981) 817–821.
[23] R.L. Seliger, I. On the breaking of nonlinear dispersive waves. II. Variational principles in continuum mechanics, Ph.D. Thesis, California Institute of Technology, 1968.
[24] A. Constantin, J. Escher, Wave breaking for nonlinear nonlocal shallow water equations, Acta Math. 181 (1998) 229–243.
[25] A. Constantin, W.A. Strauss, Stability of peakons, Comm. Pure Appl. Math. 53 (2000) 603–610.